

Chapter 1 DESCRIPTION

INTRODUCTION

This chapter describes the An-60 Ti analytical rotor, cells, and counterbalance. The An-60 Ti rotor, classified R, is designed for use in the Beckman Optima™ XL-A analytical ultracentrifuge. For complete operating instructions, use this manual in conjunction with the *Optima XL-A Analytical Ultracentrifuge Instruction Manual* (LXL/A-IM) and the *Optima XL Instruction Manual* (LXL-IM).

THE ROTOR

The An-60 Ti analytical rotor is a four-place titanium rotor (painted black), rated for 60 000 rpm. Three holes are for sample cells and the fourth is for the counterbalance; all are parallel to the axis of rotation. The cell holes are numbered for easy identification; see Figure 1. The holes, together with the windows in the cells, allow light to pass through the cells for spectrophotometric analysis of the material being centrifuged. A handle is attached for easier lifting of the rotor.



Figure 1. The An-60 Ti Analytical Rotor

A specially designed analytical overspeed disk is attached to the bottom of the rotor to detect rotor speeds exceeding 60 000 rpm. In addition, magnets have been inserted in the disk (between cell holes 4 and 1). A sensor in the rotor chamber is triggered by these magnets, which is used for timing the flash lamp strobe. Special

... should be taken to avoid damaging this dual-purpose disk.
 See Chapter 3: CARE AND MAINTENANCE for instructions
 on replacing the overspeed disk if it comes off or gets damaged.

The An-60 Ti rotor is warranted for 5000 runs, 5000 hours of centrifugation, or 5 years, whichever occurs first, at any speed from 3000 rpm up to maximum (see the WARRANTY).

THE CELLS

The analytical cell consists of a centerpiece, two window assemblies and a cell housing (see Figure 2). These components are designed with a special rib (key) and groove (keyway), which fit together to provide accurate alignment.

A 15-drawer storage cabinet is provided with special inserts to hold cell components and tools (see the Supply List).

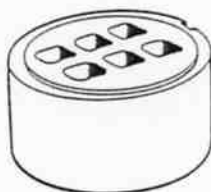
DOUBLE-SECTOR CENTERPIECES

The sample is contained in a sealed cavity formed by enclosing the centerpiece between two window assemblies. The standard centerpieces used in the An-60 Ti rotor have two cavities, which are sector shaped to minimize convection and thus reduce mixing in the cell. (These are referred to as double-sector centerpieces.) As the spinning rotor passes through the light beam, the software automatically subtracts the solvent-only absorbance in one sector from the sample-plus-solvent absorbance in the other sector, so that the data represent the absorbance of the sample only.

Centerpieces are 12 mm thick, representing the thickness of the liquid column that the light will pass through, and have a 2.5-degree sector angle (see Figure 3). For Epon centerpieces, the standard sector length is 14 mm, from cell top to cell bottom. The sector volume depends on the type of centerpiece being used (see Table 1).



Standard Centerpiece



Six-Channel Centerpiece

Figure 3. Standard and Six-Channel Equilibrium Centerpieces

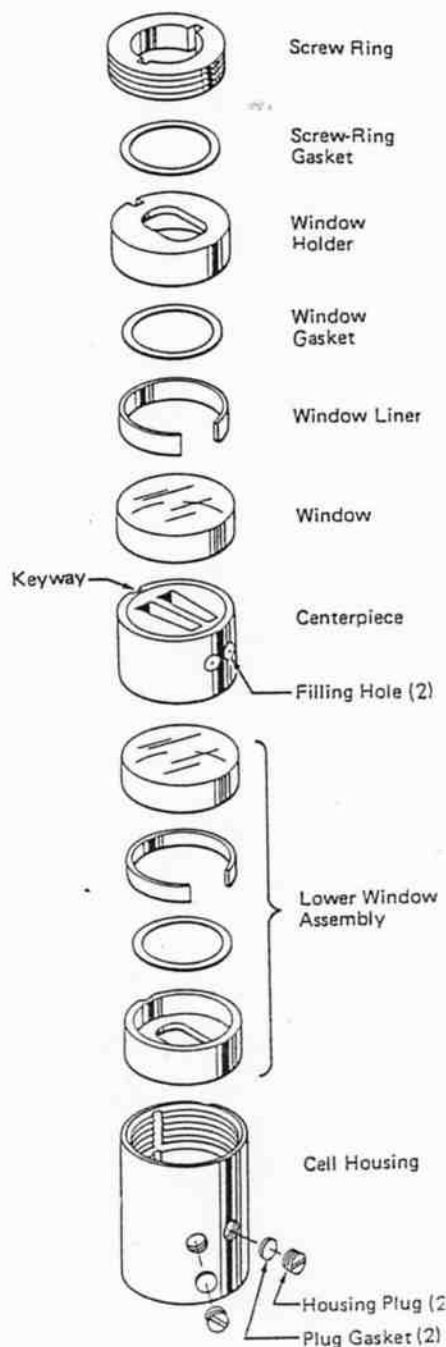


Figure 2. Exploded View of a Double-Sector Analytical Cell

ASSEMBLING STANDARD CELLS

STEP 1: ASSEMBLE WINDOWS.

- a. Place a window gasket (see Figure 6) in the window holder. (Use gaskets only a few times as they become bent or otherwise damaged with repeated use.)
- b. Place a liner in the window holder, over the gasket, with the gap in the liner *opposite* (i.e., 180 degrees) from the keyway.
- c. Hold the window with a lintless tissue and carefully insert it into the holder, aligning the mark with the keyway. (It helps to drop the window in at a slight angle, starting at the keyway.) **MAKE SURE THAT NO FINGERPRINTS OR SMUDGES GET ON THE WINDOW.**
- d. Repeat instructions *a* through *d* for the second window assembly.

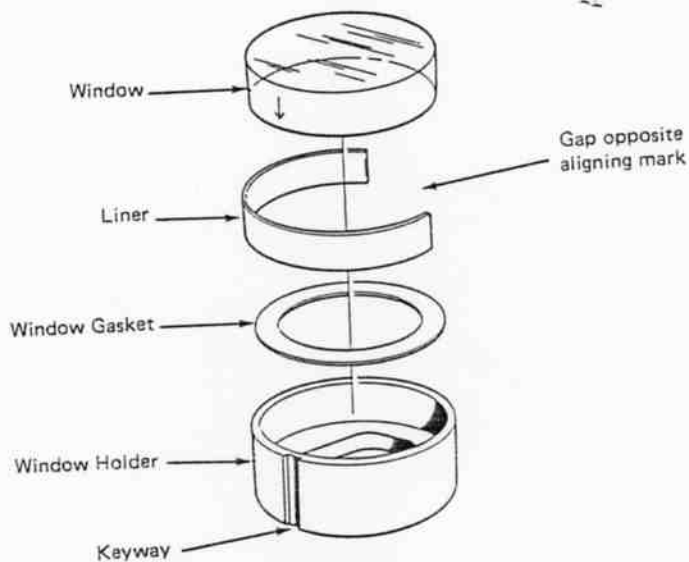


Figure 6. Assembling Window Components

If you are using band-forming centerpieces, refer to Step 5 below before proceeding. (In this case, you fill the centerpiece first.) If you are using equilibrium centerpieces, refer to the special instructions following this section.

STEP 2: STACK THE CENTERPIECE AND WINDOW ASSEMBLIES.

- a. *Double check that all cell components are scrupulously clean—to prevent leakage or damage to the centerpieces.*
- b. With the keyways aligned, stack the components in this order: window assembly on the bottom (window up), centerpiece² in the middle (capillaries facing down

² Use a red polyethylene gasket (p/n 330446) between each face of the aluminum centerpiece (p/n 334623) and window assemblies.

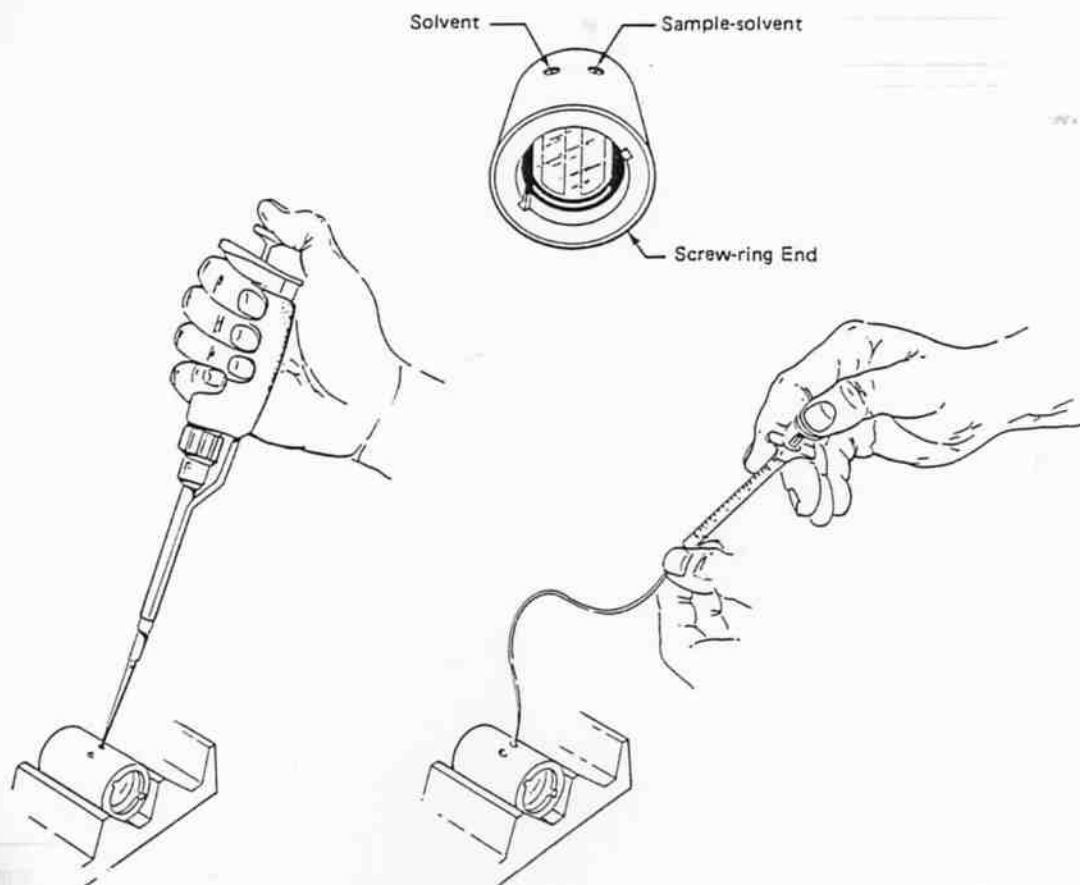


Figure 10. Filling a Standard Double-Sector Centerpiece
Using a Syringe and Hamilton Tubing

- b. If the procedure being used requires that measurements be made at the sector bottom, insert 0.05 mL of 3M's FC-43 oil into the sample sector and 0.035 mL of oil into the reference sector. (Materials such as carbon tetrachloride or Dow Corning's No. 550 silicone oil can also be used.) This base fluid will form a bottom meniscus in the cell during centrifugation. (The base fluid allows for absorbance measurements at the bottom of the solution column. If base fluid is not used, the bottom of the solution column may be partially obscured.)
- *Standard double-sector centerpieces.* Each sector holds a maximum volume of 0.45 mL. Hold the cell horizontally with the screw-ring end toward you and the filling holes up. Fill the reference (left) sector with solvent; fill the sample (right) sector with sample-solvent mixture (see Figure 10). Use a greater total volume in the reference sector so that the sample meniscus is easily recognized.
 - *Synthetic boundary capillary-type centerpieces:* The centerpiece should be placed in the housing with the capillaries up. Load the centerpiece as described above for standard centerpieces. Fill the reference (left) sector

SPECIFICATIONS

Maximum speed	60 000 rpm
Number of rotor holes (3 for sample cells; 1 for counterbalance)	4
Relative Centrifugal Field* at maximum speed	
At cell center	$262\,000 \times g$
At r_{\max} of the cell sector	$290\,000 \times g$
Approximate acceleration time to maximum speed	3 1/2 min
Approximate deceleration time from maximum speed to zero	3 1/2 min
Available centerpieces	see Table 1
Rotor operating temperature range	0 to 40°C
Rotor material	titanium
Rotor classification	R

* Relative Centrifugal Field (RCF) is the ratio of the centrifugal acceleration at a specified radius and speed ($r\omega^2$) to the standard acceleration of gravity (g) according to the following formula:

$$\text{RCF} = \frac{r\omega^2}{g}$$

where r is the radius in millimeters, ω is the angular velocity in radians per second ($2\pi \text{ RPM}/60$), and g is the standard acceleration of gravity (9807 mm/s^2). After substitution:

$$\text{RCF} = 1.12r \left(\frac{\text{RPM}}{1000} \right)^2$$

Effects of shape on translational frictional properties

Most macromolecules of biological interest are not spheres. A significant fraction appear to be compact, globular, or irregular rigid bodies. For these, an ellipsoid of revolution is a more realistic model than a sphere. There are two classes of such ellipsoids, both of which are limiting cases of the general ellipsoid with three different axes (see Fig. 10-10). The oblate ellipsoid is a disk shape, generated by rotating an ellipse around its short semiaxis b ; the two long semiaxes, a , are identical. A prolate ellipsoid is a rodlike shape, generated by rotating an ellipse around its long semiaxis a ; here the two shorter semiaxes, b , are identical. For either kind of ellipsoid, the axial ratio (p_r) is defined as a/b , the ratio of the long to the short semiaxes.

The volume of a sphere is $(4/3)\pi r^3$, whereas that of an ellipsoid is either $(4/3)\pi a^2 b$ (oblate) or $(4/3)\pi a b^2$ (prolate). For equal volumes, the surface area of either ellipsoid will be greater than that of a sphere. It seems reasonable to guess that ellipsoids will have larger frictional coefficients than equivalent spheres, and this guess is confirmed by detailed calculations. Because the volume of a molecule is proportional to the molecular weight (Eqn. 10-11), we see that (for constant mass) the more a molecule deviates from a sphere, the larger its frictional coefficient will become.

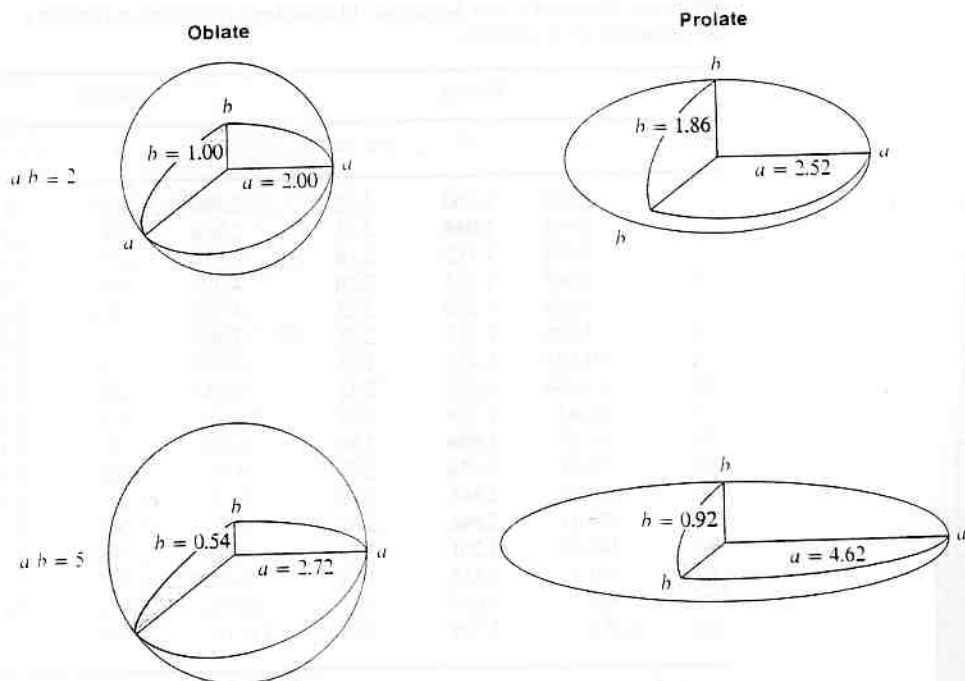


Figure 10-10

Four ellipsoids of revolution, with equal volumes. The near right octant of each ellipsoid has been cut away to show the major (a) and minor (b) axes.

For stick boundary conditions, it is possible to obtain analytical expressions for the dependence of the frictional coefficient of an ellipsoid on the axial ratio. It is useful to express these as the ratio of the frictional coefficient of an ellipsoid (f) to that of a sphere with equal volume (f_{sph}). For translational friction, the results are the following:

$$F = f/f_{\text{sph}} = (1 - p^2)^{1/2}/p^{2/3} \ln\{[1 + (1 - p^2)^{1/2}]/p\}$$

for a prolate ellipsoid, where $p = b/a = 1/p_r$ (10-19a)

$$F = f/f_{\text{sph}} = (p^2 - 1)^{1/2}/p^{2/3} \tan^{-1}[(p^2 - 1)^{1/2}]$$

for an oblate ellipsoid, where $p = a/b = p_r$ (10-19b)

These equations are not especially convenient to use; therefore, Table 10-2 lists numerical values. The translational frictional coefficient ratio F is often called a shape factor or Perrin factor. Note that the value of these factors increases rather gradually with increasing axial ratio (Fig. 10-11). Prolate ellipsoids always show a higher frictional coefficient than oblate ellipsoids of the same axial ratio. Note that,

Table 10-2

Simha (v), Perrin (F), and Scheraga-Mandelkern (β) shape parameters for ellipsoids of revolution

Axial ratio	Prolate			Oblate		
	v	F	$\beta \times 10^{-6}$	v	F	$\beta \times 10^{-6}$
1	2.500	1.000	2.12	2.500	1.000	2.12
2	2.908	1.044	2.13	2.854	1.042	2.12
3	3.685	1.112	2.16	3.430	1.105	2.13
4	4.663	1.182	2.20	4.059	1.165	2.13
5	5.806	1.250	2.23	4.708	1.224	2.14
6	7.098	1.314	2.28	5.367	1.277	2.14
8	10.103	1.433	2.35	6.700	1.374	2.14
10	13.634	1.543	2.41	8.043	1.458	2.14
15	24.65	1.784	2.54	11.42	1.636	2.14
20	38.53	1.996	2.64	14.80	1.782	2.15
30	74.51	2.356	2.78	21.58	2.020	2.15
40	120.76	2.668	2.89	28.37	2.212	2.15
50	176.81	2.946	2.97	35.16	2.375	2.15
60	242.28	3.201	3.04	41.95	2.518	2.15
80	400.5	3.658	3.14	55.52	2.765	2.15
100	593.7	4.067	3.22	69.10	2.974	2.15
200	2,052.9	5.708	3.48	137.01	3.735	2.15

NOTE: F is calculated by using Equation 10-19; v and β are calculated as described in Chapter 12 (see Eqns. 12-23 and 12-29).

SOURCE: After H. A. Scheraga, *Protein Structure* (New York: Academic Press 1961).

Sedimentation of Particles in a Gravitational Field*

When a solute particle is suspended in a solvent and subjected to a gravitational field, three forces act on the particle (Figure 1).

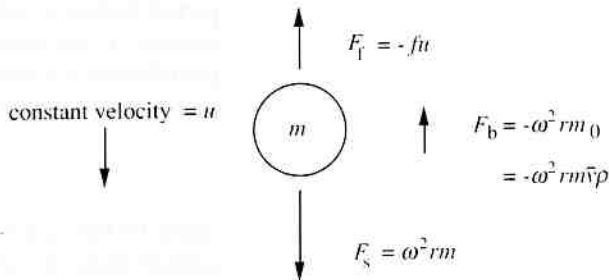


Figure 1. The forces acting on a solute particle in a gravitational field

First, there is a sedimenting, or gravitational force, F_s , proportional to the mass of the particle and the acceleration. In a spinning rotor, the acceleration is determined by the distance of the particle from the axis of rotation, r , and the square of the angular velocity, ω (in radians per second).

$$F_s = m\omega^2 r = \frac{M}{N} \omega^2 r \quad (1)$$

where m is the mass in grams of a single particle, M is the molar weight of the solute in g/mol and N is Avogadro's number. (Note that the molecular weight is numerically equal to the molar weight, but is dimensionless.)

Second, there is a buoyant force, F_b , that, from Archimedes' principle, is equal to the weight of fluid displaced:

$$F_b = -m_0 \omega^2 r \quad (2)$$

*The following discussion is made in terms of a simple mechanical model of sedimentation. Some of the ambiguities that arise from this type of treatment can be avoided by use of a thermodynamic approach (Tanford, 1961).

where m_0 is the mass of fluid displaced by the particle:

$$m_0 = m\bar{v}\rho = \frac{M}{N}\bar{v}\rho \quad (3)$$

Here, \bar{v} is the volume in mL that each gram of the solute occupies in solution (the *partial specific volume*; the inverse of its effective density) and ρ is the density of the solvent (g/mL). Provided that the density of the particle is greater than that of the solvent, the particle will begin to sediment. As the particle begins to move along a radial path towards the bottom of the cell, its velocity, u , will increase because of the increasing radial distance. Since particles moving through a viscous fluid experience a frictional drag that is proportional to the velocity, the particle will experience a frictional force:

$$F_f = -fu \quad (4)$$

where f is the frictional coefficient, which depends on the shape and size of the particle. Bulky or elongated particles experience more frictional drag than compact, smooth spherical ones. The negative signs in equations (2) and (4) indicate that these two forces act in the opposite direction to sedimentation.

Within a very short time (usually less than 10^{-6} s) the three forces come into balance:

$$F_s + F_b + F_f = 0 \quad (5)$$

$$\frac{M}{N}\omega^2r - \frac{M}{N}\bar{v}\rho\omega^2r - fu = 0 \quad (6)$$

Rearranging:

$$\frac{M}{N}(1 - \bar{v}\rho)\omega^2r - fu = 0 \quad (7)$$

Collecting the terms that relate to the particle on one side, and those terms that relate to the experimental conditions on the other, we can write:

$$\frac{M(1 - \bar{v}\rho)}{Nf} = \frac{u}{\omega^2r} \equiv s \quad (8)$$

The term u/ω^2r , the velocity of the particle per unit gravitational acceleration, is called the *sedimentation coefficient*, and can be seen to depend on the properties of the particle. In particular, it is proportional to the buoyant effective molar weight of the particle (the molar weight corrected for the

effects of buoyancy) and it is inversely proportional to the frictional coefficient. *It is independent of the operating conditions.* Molecules with different molecular weights, or different shapes and sizes, will, in general, move with different velocities in a given centrifugal field; *i.e.*, they will have different sedimentation coefficients.

The sedimentation coefficient has dimensions of *seconds*. For many substances, the value of s lies between 1 and 100×10^{-13} seconds. The Svedberg unit (abbreviation S) is defined as 10^{-13} seconds, in honor of Thé Svedberg. Serum albumin, then, has a sedimentation coefficient of 4.5×10^{-13} seconds or 4.5 S.

As the process of sedimentation continues, the solute begins to pile up at the bottom of the centrifuge cell. As the concentration at the bottom begins to increase, the process of *diffusion* opposes that of sedimentation. After an appropriate period of time, the two opposing processes approach equilibrium in all parts of the solution column and, for a single, ideal solute component, the concentration of the solute increases exponentially towards the cell bottom. At sedimentation equilibrium, the processes of sedimentation and diffusion are balanced; the concentration distribution from the top of the cell to the bottom no longer changes with time, and is a function of molecular weight.

As indicated above, the process of sedimentation depends on the *effective* molar weight, corrected for the buoyancy: $M(1 - \bar{v}\rho)$. If the density of the solute is greater than that of the solvent, the solute will sediment towards the cell bottom. However, if the density of the solute is less than that of the solvent, the solute will float towards the meniscus at the top of the solution. This is the situation for many lipoproteins and lipids in aqueous solutions. The analysis of such situations is similar, except that the direction of movement is reversed.

When the densities of the solute and solvent are equal, $(1 - \bar{v}\rho) = 0$, and there will be no tendency to move in either direction. Use can be made of this to determine the density of a macromolecule in *density gradient sedimentation*. A gradient of density can be made, for example by generating a gradient of concentration of an added solute such as sucrose or cesium chloride from high concentrations at the cell bottom to lower values at the top. The macromolecule will sediment if it is in a region of solution where the density is less than its own. But macromolecules that find themselves in a region of higher density will begin to float. Eventually, the macromolecules will form a layer at that region of the cell where the solvent density is equal to their own: the buoyant density.

Instrumentation

An analytical ultracentrifuge must spin a rotor at an accurately controlled speed and at an accurately controlled temperature, and must allow the recording of the concentration distribution of the sample at known times. This ability to measure the distribution of the sample while it is spinning sets the analytical ultracentrifuge apart from preparative centrifuges.

In order to achieve rapid sedimentation and to minimize diffusion, high angular velocities may be necessary. The rotor of an analytical ultracentrifuge is typically capable of rotating at speeds up to 60,000 rpm. In order to minimize frictional heating, and to minimize aerodynamic turbulence, the rotor is usually spun in an evacuated chamber. It is important that the spinning rotor be stable and free from wobble or precession. Instability can cause convection and stirring of the cell contents, particularly when the concentration and concentration gradient of the solute are low, and can lead to uncertainty in the concentration distribution in regions of high concentration gradient.

Rotors

Rotors for analytical ultracentrifugation must be capable of withstanding enormous gravitational stresses. At 60,000 rpm, a typical ultracentrifuge rotor generates a centrifugal field in the cell of about $250,000 \times g$. Under these conditions, a mass of 1 g experiences an apparent weight of 250 kg; *i.e.*, $\frac{1}{4}$ ton! The rotor must also allow the passage of light through the spinning sample, and some mechanism must be available for temperature measurement.

The Optima™ XL-A Analytical Ultracentrifuge is equipped with a four-hole rotor. One of the holes is required for the *counterbalance*, with its reference holes that provide calibration of radial distance, leaving three positions available for sample cells. Operation with multiple cells increases the number of samples that can be examined in a single experiment. This is particularly useful, for example, when several different concentrations of a self-associating material must be examined in order to check for attainment of chemical equilibrium.

Cells

Ultracentrifuge cells must also withstand the stresses caused by the extremely high gravitational fields, must not leak or distort, and yet must allow the passage of light through the sample so that the concentration distribution can be measured. To achieve these ends, the sample is usually contained within a sector-shaped cavity sandwiched between two thick windows of optical-grade quartz or sapphire. The cavity is produced in a *centerpiece* of aluminum alloy, reinforced epoxy, or a polymer known as Kel-F.* Double-sector centerpieces for the Optima XL-A are available with optical lengths of 3 and 12 mm. User-manufactured centerpieces have been reported with pathlengths as short as 0.1 mm (Braswell *et al.*, 1986; Brian *et al.*, 1981; Minton and Lewis, 1981; Murthy *et al.*, 1988). The combination of various optical pathlengths and selectable wavelengths allows examination of a wide range of sample concentrations.

Sector-shaped sample compartments are essential in velocity work since the sedimenting particles move along radial lines. If the sample compartments were parallel-sided, sedimenting molecules at the periphery would collide with the walls and cause convective disturbances. Sectors that diverge more widely than the radii also cause convection. The development of appropriate sector-shaped sample compartments with smooth walls was a major factor in Svedberg's successful design of the original velocity instrument.

Double-sector cells allow the user to take account of absorbing components in the solvent, and to correct for the redistribution of solvent components, particularly at high g values. A sample of the solution is placed in one sector, and a sample of the solvent in dialysis equilibrium with the solution is placed in the second sector (Figure 2). The optical system measures the difference in absorbance between the sample and reference sectors in a manner similar to the operation of a double-beam spectrophotometer. Double-sector cells also facilitate measurements of differences in sedimentation coefficient, and of diffusion coefficients.

*A registered trademark of 3M.

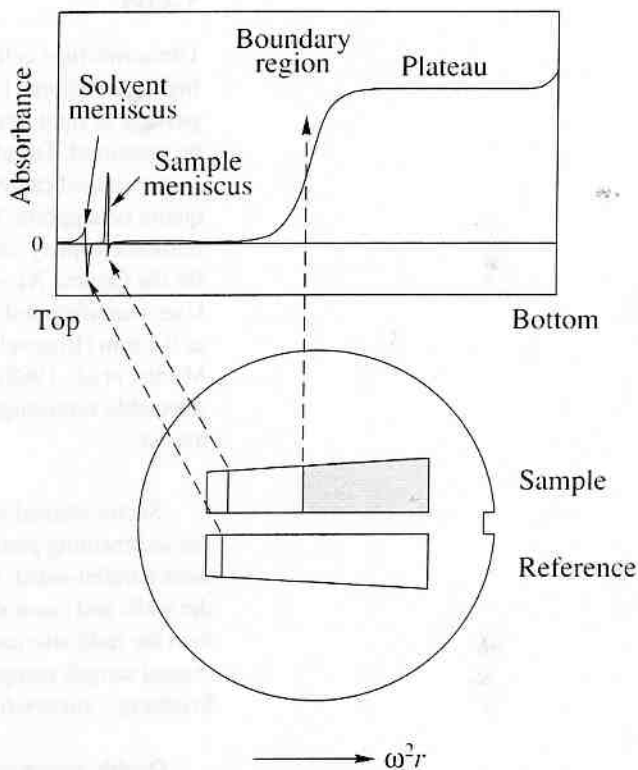


Figure 2. Double-sector centerpiece. The sample solution is placed in one sector, and a sample of the solvent in dialysis equilibrium with the sample is placed in the reference sector. The reference sector is usually filled slightly more than the sample sector, so that the reference meniscus does not obscure the sample profile.

In equilibrium experiments, the time required to attain equilibrium within a specified tolerance is decreased for shorter column lengths of solution; *i.e.*, when the distance from the meniscus to the cell bottom is only 1 to 3 mm, rather than the 12 mm or so for a full sector. Considerable savings of time can be achieved by examining 3 samples at once in 6-channel centerpieces, in which 3 channels hold 3 different samples, and the 3 channels on the other side hold the respective dialyzed solvents (Yphantis, 1964). For even more rapid attainment of equilibrium, 1-mm solution lengths may be used (Arakawa *et al.*, 1991; Van Holde and Baldwin, 1958).

Absorbance

While earlier absorption optical systems (Figure 3c) suffered from the disadvantage of requiring photography and subsequent densitometry of the photograph, the photoelectric scanners of older instruments allowed more direct collection of data onto chart recorder paper. The primary data again had to be transcribed for calculations, a tedious and error-prone process.

With the advent of the Optima XL-A, however, many of these problems seem to have been solved. The instrument possesses increased sensitivity and wide wavelength range; with its high reproducibility, baseline scans may be subtracted to remove the effects of oil droplets on lenses and windows, and of optical imperfections in the windows and lenses. With the absorbance optics, too, the *absolute* concentration is available in principle at any point (Figure 3d); we are not restricted to concentration *difference* with respect to reference points, and accurate accounting is not a prerequisite for determining absolute concentrations.

The absorbance optical system of the Optima XL-A is shown in Figure 4. A high-intensity xenon flash lamp allows the use of wavelengths between 190 and 800 nm. The lamp is fired briefly as the selected sector passes the detector. Cells and individual sectors may be examined in turn, with the aid of timing information from a reference magnet in the base of the rotor. The measured light is normalized for variation in lamp output by sampling a reflected small fraction of the incident light.

A slit below the sample moves to allow sampling of different radial positions. To minimize noise, multiple readings at a single position may be collected and averaged. A new and as yet not fully explored capability of the absorbance optics is the wavelength scan. A wavelength scan may be taken at a specified radial position in the cell, resulting in an absorbance spectrum of the sample at that point, and allowing discrimination between different solutes.

The increased sensitivity of the absorbance optics means that samples may be examined in concentrations too dilute for schlieren or interference optics. With proteins, for example, measurement below 230 nm allows examination of concentrations 20 times more dilute than can be studied with interference optics (*i.e.*, concentrations as low as several $\mu\text{g/mL}$ are now accessible). Accessibility to lower concentrations means that examination of stronger interactions ($K > 10^7 \text{ M}^{-1}$) is now possible.

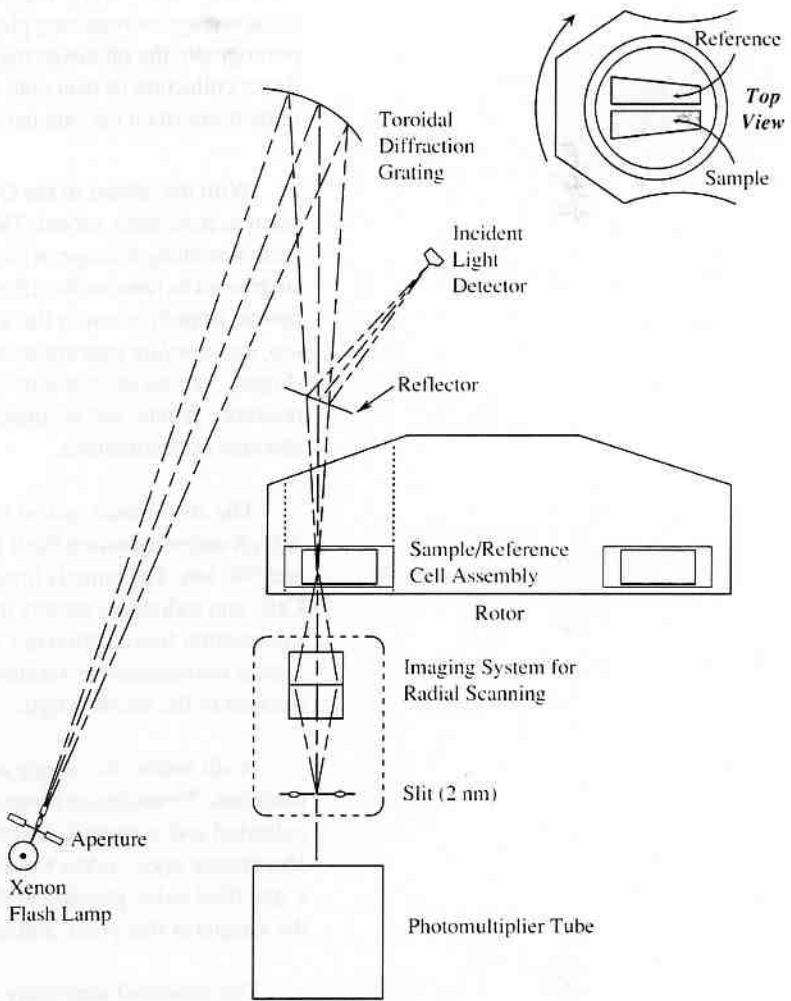


Figure 4. Schematic diagram of the optical system of the Beckman Optima XL-A Analytical Ultracentrifuge

Sedimentation Velocity

There are two basic types of experiment with the analytical ultracentrifuge: sedimentation velocity and sedimentation equilibrium.

In the more familiar sedimentation velocity experiment, an initially uniform solution is placed in the cell and a sufficiently high angular velocity is used to cause relatively rapid sedimentation of solute towards the cell bottom. This produces a depletion of solute near the meniscus and the formation of a sharp boundary between the depleted region and the uniform concentration of sedimenting solute (the *plateau*; see Figures 2 and 3). Although the velocity of individual particles cannot be resolved, the rate of movement of this boundary (Figure 5) can be measured. This leads to the determination of the sedimentation coefficient, s , which depends directly on the mass of the particles and inversely on the frictional coefficient, which is in turn a measure of effective size (see equation 8).

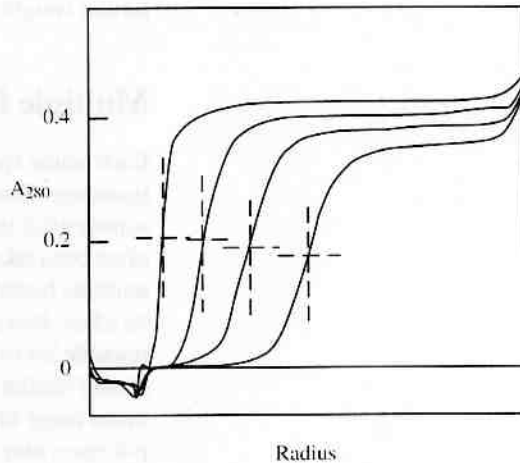


Figure 5. Movement of the boundary in a sedimentation velocity experiment with a recombinant malaria antigen protein. As the boundary progresses down the cell, the concentration in the plateau region decreases from radial dilution, and the boundary broadens from diffusion. The midpoint positions, r_{mid} , of the boundaries are indicated.

Measurement of the rate of spreading of a boundary can lead to a determination of the *diffusion coefficient*, D , which depends on the effective size of the particles:

$$D = \frac{RT}{Nf} \quad (10)$$

where R is the gas constant and T the absolute temperature. The ratio of the sedimentation to diffusion coefficient gives the molecular weight:

$$M = \frac{s^0 RT}{D^0(1 - \bar{v}\rho)} \quad (11)$$

where M is the molar weight of the solute, \bar{v} its partial specific volume, and ρ is the solvent density. The superscript zero indicates that the values of s and D , measured at several different concentrations, have been extrapolated to zero concentration to remove the effects of interactions between particles on their movement. Less accurately, for a particular class of macromolecule (*e.g.*, globular proteins or DNA), empirical relationships between the sedimentation coefficient and molecular weight may allow estimation of approximate molecular weights from very small samples (Freifelder, 1970; Van Holde, 1975).

Multiple Boundaries

Each solute species in solution in principle gives rise to a separate sedimenting boundary. Thus, the existence of a single sedimenting boundary (or a single, symmetrical bell-shaped "peak" of dc/dr as seen with schlieren optics) has often been taken as evidence for homogeneity. Conversely, the existence of multiple boundaries is evidence for multiple sedimenting species. Care must be taken, however, in making inferences concerning homogeneity. It may be possible for two separate species to have sedimentation coefficients sufficiently similar that they cannot clearly be resolved. Furthermore, the relatively broad range of molecular weights present in preparations of many synthetic polymers may lead to a single boundary. This boundary, however, will show more spreading during the experiment than expected from the size of the particles. It is possible to take account of this type of behavior as discussed in a later section.

Conversely, it is possible for a pure solute component to produce multiple sedimenting boundaries, for example, by the existence of several stable aggregation states. This type of effect depends on how rapidly the different states can interconvert. If the interconversion is rapid in the time scale of the

experiment, the distribution of the different boundaries may be uniquely dependent on the solute concentration. On the other hand, if re-equilibration is slow, the proportion of the different species may reflect the past history of the sample rather than the concentration in the cell.

Determination of s

Provided that the sedimenting boundary is relatively sharp and symmetrical, the rate of movement of solute molecules in the plateau region can be closely approximated by the rate of movement of the midpoint, r_{bnd} . This point, in turn, is very close to the position of the point of inflection (which is the same as the maximum ordinate, or "peak," of the dc/dr curve).

Since the sedimenting force is not constant, but increases with r , the velocity of the boundary will increase gradually with movement of the boundary outwards, so the velocity must be expressed as a differential:

$$s \equiv \frac{u}{\omega^2 r} = \frac{dr_{\text{bnd}}/dt}{\omega^2 r} \quad (12)$$

Whence:

$$\ln(r_{\text{bnd}}/r_m) = s\omega^2 t \quad (13)$$

where r_m is the radial position of the meniscus.

A plot of $\ln r_{\text{bnd}}$ versus time in seconds yields a straight line of slope $s\omega^2$ (Figure 6). When the boundary is asymmetric, or imperfectly resolved from the meniscus, it can be shown that the square root of the second moment of the concentration distribution, \bar{r} , is an accurate measure of the movement of particles in the plateau region (Goldberg, 1953; Schachman, 1959):

$$\bar{r}^2 = r_p^2 - \frac{2}{c_p} \int_{r_m}^{r_p} cr dr \quad (14)$$

where \bar{r} is the *equivalent boundary position*, and r_p is a position in the plateau region with concentration c_p . This method also yields the *weight-average sedimentation coefficient* of mixtures or interacting systems, and it is a simple matter to evaluate the integral numerically when the data are collected by a computer.

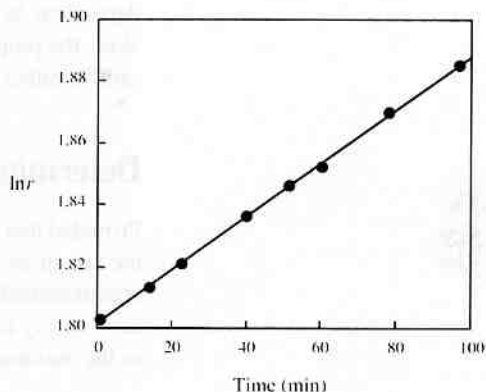


Figure 6. Plot of the logarithm of the radial position, r_{bnd} , of a sedimenting boundary as a function of time for recombinant dihydroorotase domain protein. The slope of this plot yields the sedimentation coefficient. (Unpublished data of N. Williams, K. Seymour, P. Yin, R. I. Christopherson and G. B. Ralston.)

Solvent Effects

The sedimentation coefficient is influenced by the density of the solvent and by the solution viscosity. In order to take into account the differences in density and viscosity between different solvents, it is conventional to calculate sedimentation coefficients in terms of a standard solvent, usually water at 20°C:

$$s_{20,w} = s_{obs} \left(\frac{\eta_{T,w}}{\eta_{20,w}} \right) \left(\frac{\eta_s}{\eta_w} \right) \left(\frac{1 - \bar{v}\rho_{20,w}}{1 - \bar{v}\rho_{T,s}} \right) \quad (15)$$

where $s_{20,w}$ is the sedimentation coefficient expressed in terms of the standard solvent of water at 20°C; s_{obs} is the measured sedimentation coefficient in the experimental solvent at the experimental temperature, T ; $\eta_{T,w}$ and $\eta_{20,w}$ are the viscosities of water at the temperature of the experiment and at 20°C, respectively; η_s and η_w are, respectively, the viscosities of the solvent and water at a common temperature; $\rho_{20,w}$ is the density of water at 20°C and $\rho_{T,s}$ is that of the solvent at the temperature of the experiment.

Sedimentation Equilibrium

In sedimentation equilibrium experiments, a small volume of an initially uniform solution is centrifuged at a somewhat lower angular velocity than is required for a sedimentation velocity experiment. As solute begins to sediment towards the cell bottom and the concentration at the bottom increases, the process of diffusion opposes the process of sedimentation. After an appropriate period of time, the two opposing processes approach equilibrium (Figure 14), and the concentration of the solute increases exponentially towards the cell bottom. At equilibrium the resultant solute distribution is invariant with time. Measurement of the concentration at different points leads to the determination of the molar weight of the sedimenting solute (numerically equal to the molecular weight).

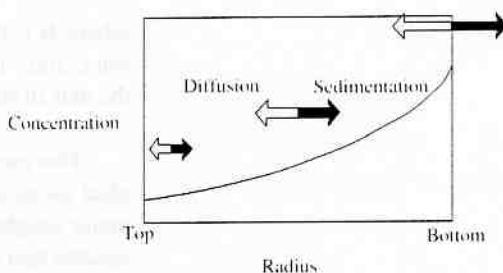


Figure 14. Schematic representation of sedimentation equilibrium. The flow of solute due to sedimentation (black arrows) increases with radial distance. This process is balanced at equilibrium by the reverse flow from diffusion (open arrows), which increases with concentration gradient. At equilibrium, the resulting concentration distribution is exponential with the square of the radial position.

The time required to reach equilibrium depends on the square of the length of the solution column in the radial direction: for a solution column 3 mm long that attains equilibrium in 18 hours, a 1-mm solution column will come to equilibrium in approximately 2 hours. For a 3-mm column length in a standard 12-mm double-sector cell, 120 μL are required. A 1-mm column length requires only 40 μL .

The most rigorous approach to analysis of sedimentation equilibrium is through the application of thermodynamics (Williams *et al.*, 1958): at equilibrium, the *total* potential of solute is the same at all points in the cell. From a simpler, mechanical point of view, at equilibrium there is no net movement of molecules, so diffusional flow exactly balances sedimentation flow everywhere in the cell. Because the sedimentation flow is proportional to $\omega^2 r$, and r increases towards the cell bottom, there must be a greater sedimenting tendency at the bottom of the cell. Consequently, there must be a greater balancing tendency for diffusion in the opposite direction. Because diffusion is driven by the *gradient of chemical potential* (which is dependent on the concentration gradient), it follows that the concentration gradient increases towards the cell bottom. It can be shown that, for a single, ideal, nonassociating solute:

$$M = \frac{2RT}{(1 - \bar{v}\rho)\omega^2} \times \frac{d(\ln c)}{dr^2} \quad (26)$$

where M is the solute molar weight (in g/mol), ω the angular velocity of the rotor, and c the concentration of the solute (in g/L) at a radial distance r from the axis of rotation.

This means that a plot of $\log(\text{concentration})$ *versus* $(\text{radius})^2$ for a single, ideal solute at sedimentation equilibrium yields a slope proportional to the molar weight. Alternatively, one can fit the data of c *versus* r^2 to find the least squares best estimate of $M/(1 - \bar{v}\rho)$.

The sedimentation equilibrium experiment is still the best way for determining the molecular weights of macromolecules. It is applicable to a wide range of molecular sizes, from sucrose ($M_r = 360$; Van Holde and Baldwin, 1958) to viruses ($M_r =$ many millions; Bancroft and Freifelder, 1970). For low molecular weight solutes, high angular velocities are required: the lower limit of molecular weight measurable depends on the maximum speed capable with the rotor or centrifuge. The upper limit of molecular weight depends on the stability of the rotor at low speeds, and the width of the meniscus. The high stability of the drive system of the Optima XL-A enables lower speeds (as low as 1,000 rpm) to be used with some confidence, and hence raises the upper limit of measurable molecular weight. At very low speeds, however, the solution meniscus is no longer nearly vertical, but displays more marked curvature as the centrifugal gravitational field decreases to become comparable with the earth's gravitational field (Figure 15).